

# Performance Limitations of Wide-Gap (Ag,Cu)(In,Ga)Se<sub>2</sub> Thin-Film Solar Cells

Jan Keller,\* Patrick Pearson, Nina Shariati Nilsson, Olof Stolt, Lars Stolt, and Marika Edoff

The effect of absorber stoichiometry in (Ag,Cu)(In,Ga)Se<sub>2</sub> (ACIGS) solar cells with bandgaps ( $E_g$ ) > 1.40 eV is studied on a large sample set. It is confirmed that moving away in composition from ternary AgGaSe<sub>2</sub> by simultaneous reduction in Ga and Ag content widens the chalcopyrite single-phase region and thereby reduces the amount of ordered vacancy compounds (OVCs). As a consequence, a distortion in current–voltage characteristics, ascribed to OVCs at the back contact, can be successfully avoided. A clear anticorrelation between open-circuit voltage ( $V_{OC}$ ) and short-circuit current density ( $J_{SC}$ ) is detected with varying absorber stoichiometry, showing decreasing  $V_{OC}$  and increasing  $J_{SC}$  values for  $[I]/[III] > 0.9$ . Capacitance profiling reveals that the absorber doping gradually decreases toward stoichiometric composition, eventually leading to complete depletion. It is observed that only such fully depleted samples exhibit perfect carrier collection, evidencing a very low diffusion length in wide-gap ACIGS films. The results indicate that OVCs at the surface play a minor or passive role for device performance. Finally, a solar cell with  $V_{OC} = 0.916$  V at  $E_g = 1.46$  eV is measured, which is, to the best of our knowledge, the highest value reported for this bandgap to date.

module, thereby minimizing dead area and resistive losses. For  $E_g > 1.4$  eV, the absorber material eventually becomes interesting for utilization in a top cell of a tandem device. While bandgap values > 1.55 eV are needed to exceed theoretical efficiency values of 40% in a two-terminal configuration (bottom cell  $E_g < 1$  eV), this is already the case for  $E_g > 1.4$  eV in a tandem with four terminals (bottom cell  $E_g < 1.1$  eV).<sup>[4,5]</sup>

Despite a considerable effort in the research community,<sup>[6]</sup> the efficiency gap between low- and wide-gap CIGS solar cells could not be significantly narrowed, yet. The most crucial issue is the increasing  $V_{OC}$  deficit with respect to the bandgap energy when the GGI value exceeds 0.3 (i.e.,  $E_g > 1.2$  eV).<sup>[7]</sup> It is still under debate as to how much of this  $V_{OC}$  loss is caused by recombination at the buffer/absorber interface and how much by


Shockley–Read–Hall (SRH) recombination in the bulk. Several studies suggest that the CIGS bulk properties deteriorate with increasing GGI > 0.3. The most discussed origin is the Ga<sub>Cu</sub> antisite donor defect, which becomes energetically deeper and thus, a more effective recombination center, with increasing GGI value.<sup>[8–11]</sup> It was further found that the density of deep acceptor states increases for GGI > 0.25<sup>[12,13]</sup> and that grain boundaries are more likely to be Cu enriched (supposedly detrimental<sup>[14]</sup>) for GGI > 0.4.<sup>[15]</sup> Finally, it was suggested that the defect density in the absorber increases for GGI > 0.2, due to an increasing tetragonal distortion of the CIGS lattice.<sup>[16]</sup>

Apart from potentially inferior bulk properties of wide-gap CIGS, interface recombination was shown to be dominant for Cu-rich absorbers with GGI > 0.5, due to a negative conduction band offset (CBO) at the CdS/CIGS interface (“cliff”),<sup>[17]</sup> which reduces type inversion and thereby enhances recombination.<sup>[18,19]</sup> Other studies suggest that the high doping in Cu-rich absorbers may enhance interface recombination by tunneling.<sup>[20,21]</sup> In contrast, commonly used Cu-poor absorbers were suggested to be limited by bulk recombination, as the presence of a thin and fully covering ordered vacancy compound (OVC) is claimed to cancel out interface recombination by repelling holes from the buffer.<sup>[18,19]</sup> In contrast, the application of alternative buffer layers like (Zn,Sn)O, for which the electron affinity ( $\chi$ ) is adjusted to form a positive CBO (“spike”) to the absorber, leads to a significant  $V_{OC}$  boost in Cu-poor wide-gap devices.<sup>[22,23]</sup> This

## 1. Introduction

Today, highest conversion efficiencies ( $\eta$ ) of Cu(In,Ga)Se<sub>2</sub> (CIGS) solar cells are reached for absorber bandgap energies ( $E_g$ ) below 1.2 eV, peaking at  $\eta = 22.6\%$ <sup>[1]</sup> and  $\eta = 23.4\%$ <sup>[2]</sup> if sulfur is incorporated. Increasing the bandgap is interesting for several reasons. First of all, the global optimum lies at a slightly higher value of  $E_g = 1.34$  eV,<sup>[3]</sup> which requires [Ga]/([Ga]+[In]) (GGI) values of about 0.5, as compared with GGI  $\approx$  0.3 for the record CIGS device.<sup>[1]</sup> Another benefit of widening the bandgap is the potentially increased open-circuit voltage ( $V_{OC}$ ), allowing to reduce the number of series-connected cells in a monolithic

J. Keller, P. Pearson, N. Shariati Nilsson, O. Stolt, L. Stolt, M. Edoff  
 Ångström Solar Center  
 Division of Solar Cell Technology  
 Uppsala University  
 75121 Uppsala, Sweden  
 E-mail: jan.keller@angstrom.uu.se

 The ORCID identification number(s) for the author(s) of this article can be found under <https://doi.org/10.1002/solr.202100403>.

© 2021 The Authors. Solar RRL published by Wiley-VCH GmbH. This is an open access article under the terms of the Creative Commons Attribution License, which permits use, distribution and reproduction in any medium, provided the original work is properly cited.

DOI: 10.1002/solr.202100403

strongly indicates that interface recombination is not negligible in Cu-poor CIGS/CdS solar cells with  $\text{GGI} > 0.3$  and becomes more pronounced with increasing GGI. A likely explanation is that the potentially forming OVC is not fully covering the absorber surface, but rather appears in separated patches. This would leave a certain area fraction, exhibiting a direct and detrimental, cliff-like CIGS/CdS interface.

A possible way to decrease the interface recombination in wide-gap chalcopyrite solar cells with CdS buffers is by optimizing the CBO via controlled Ag alloying, forming a quinary (Ag,Cu)(In,Ga)Se<sub>2</sub> (ACIGS) compound. Calculations within density functional theory (DFT) predict that a positive CBO at the CdS interface can be created for any GGI value by sufficient Ag addition. Thus, a spike-like configuration can be achieved for a wide range of bandgaps up to  $E_g \approx 1.8$  eV.<sup>[24]</sup> Consequently, some promising  $V_{\text{OC}}$  values (890–960 mV) could be achieved for ACIGS solar cells with  $E_g = 1.60$ – $1.75$  eV and  $[\text{Ag}]/([\text{Ag}]+[\text{Cu}])$  (AAC) ratios  $\geq 0.75$ .<sup>[25–28]</sup>

In previous studies, a substantial formation of OVCs was found for group-I (I)-deficient ACIGS within the compositional window of  $\text{GGI} > 0.5$  and  $\text{AAC} > 0.5$ .<sup>[29,30]</sup> Further investigations revealed that these OVCs are present in the form of isolated patches located at the interfaces, as a consequence of the applied three-stage deposition process.<sup>[24,28]</sup> Recently, we studied the effect of absorber stoichiometry (i.e.,  $[\text{I}]/[\text{III}]$  value) on ACIGS with constant  $\text{GGI} = 0.80$  and  $\text{AAC} = 0.85$ , resulting in  $E_g = 1.61$  eV (optimum for top cell in 2T tandem).<sup>[28]</sup> For a large off-stoichiometry ( $[\text{I}]/[\text{III}] < 0.85$ ), (Ag,Cu)(In,Ga)<sub>3</sub>Se<sub>5</sub> (1:3:5) patches were observed at the front and back contact (see top of **Figure 1**). For higher  $[\text{I}]/[\text{III}]$  values, they were only present at the front contact and further decreased in volume when approaching 1:1:2 stoichiometry. The presence of OVCs at the back contact correlates with a kink in the current–voltage ( $I$ – $V$ ) characteristics, leading to a low fill factor (FF). It was found that the OVCs strongly accumulate Na atoms,

which presumably reduces the Na concentration at the ACIGS/MoSe<sub>2</sub> interface, where it is supposedly needed to form an ohmic contact.<sup>[31,32]</sup> In addition, a deterioration in carrier collection with decreasing  $[\text{I}]/[\text{III}]$  value was observed, resulting in low short-circuit current densities ( $J_{\text{SC}}$ ) for off-stoichiometric samples. It was speculated that the OVCs at the front contact are directly responsible for the  $J_{\text{SC}}$  losses, as the presumably high CBO at their interfaces with CdS and the 1:1:2 absorber may let them act as electron traps.<sup>[17,28,33–36]</sup> In summary, it was concluded that the presence OVCs is detrimental in several aspects and they should be avoided.

Earlier investigations point to a narrowing 1:1:2 chalcopyrite single-phase region with increasing AAC and (most likely) GGI value, that is, toward pure AgGaSe<sub>2</sub>.<sup>[28,37–39]</sup> Thus, to increase the tolerance to off-stoichiometry and thereby reduce the OVC fraction, the Ag and Ga contents were lowered in the present study, with respect to our earlier work,<sup>[28]</sup> to  $\text{AAC} = 0.47$ – $0.67$  and  $\text{GGI} = 0.66$ – $0.79$ . **Figure 1** shows the bandgap and absorber conduction band minimum (CBM) with respect to pure CuInSe<sub>2</sub> as a function of ACIGS composition, as calculated by DFT (for more information see the study by Keller et al.<sup>[24]</sup>). The cliff-spike transition at the CdS interface is indicated as well, assuming a CBO of 0.3 eV between CuInSe<sub>2</sub> ( $\chi_{\text{CuInSe}_2} \approx 4.55$  eV) and CdS ( $\chi_{\text{CdS}} \approx 4.25$  eV). The compositional window investigated in this work is highlighted. Corresponding bandgap energies are in the range of  $E_g = 1.40$ – $1.49$  eV and the CBO values are all positive (40–170 meV), that is, similar to the CBO in our previous work.<sup>[28]</sup> To obtain a high statistical significance, solar cells were processed from 40 different absorber depositions. Each ACIGS run exhibited a relative, lateral spread in  $[\text{I}]/[\text{III}]$  of  $\approx 10\%$  but negligible variation in GGI and AAC. To utilize this variation in I deficiency, four samples with different stoichiometry were extracted from each absorber processing. For a more detailed description of the lateral compositional variations within each ACIGS deposition, we refer to **Figure S1**, Supporting Information. After disregarding the I-rich (“dead”) samples, a total number of 139 samples with  $[\text{I}]/[\text{III}] = 0.75$ – $1.00$  was analyzed. The quantity of data points, combined with the large and continuous spread in  $[\text{I}]/[\text{III}]$ , allows to identify clear trends in device performance with varying absorber stoichiometry. In addition, the impact of the surface OVCs is revised and discussed.

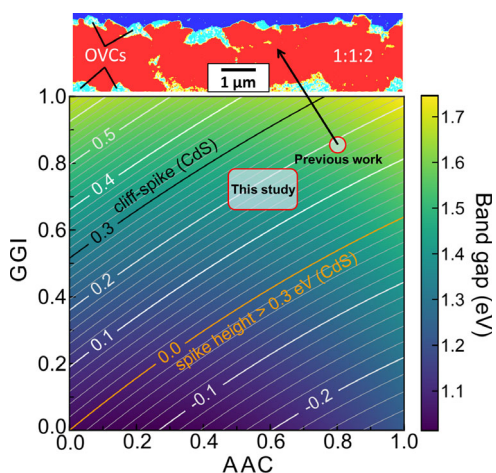


**Figure 1.** Calculated (DFT) contour lines showing ACIGS compositions with the same CBM level relative to pure CuInSe<sub>2</sub> (in eV). Corresponding calculated (DFT) bandgap energies are represented by the background color code (for more information, see the study by Keller et al.<sup>[24]</sup>). The compositional window investigated in this study is highlighted. The image at the top shows a cross-sectional  $[\text{I}]/[\text{III}]$  map of a sample from our previous work<sup>[28]</sup> with an integral composition of  $\text{AAC} = 0.80$ ,  $\text{GGI} = 0.85$ , and a large, integral off-stoichiometry ( $[\text{I}]/[\text{III}] = 0.76$ ).

## 2. Results and Discussion

The results are presented in three parts. First, the formation of OVCs is characterized and their abundance compared with samples with higher GGI and AAC values from our previous work.<sup>[28]</sup> In the second part, the standard solar cell parameters are summarized and discussed with respect to absorber composition and stoichiometry. To understand and explain the observed trends, a more detailed loss analysis is provided for an exemplary sample in the third part. Finally, the results are discussed and general conclusions for wide-gap ACIGS solar cells are summarized.

### 2.1. Width of the Chalcopyrite 1:1:2 Single-Phase Region

Raman spectroscopy is a suitable technique to identify and quantify OVCs in different chalcopyrite absorber films,<sup>[28,40–42]</sup> as the

corresponding signal can be clearly distinguished from the 1:1:2 peak. **Figure 2a** shows the OVC peak intensity relative to the 1:1:2 signal ( $A_1$  modes) as a function of  $[I]/[III]$ , as extracted from Raman measurements on selected samples with very similar compositions of  $AAC = 0.60$  ( $\pm 0.02$ ) and  $GGI = 0.72$  ( $\pm 0.02$ ). As the probing depth was about 200 nm ( $\lambda_{\text{laser}} = 532$  nm), the graph illustrates the OVC fraction at the absorber surface. Slight variations in peak ratio can be explained by a lateral inhomogeneity in phase distribution, considering a laser spot area of  $\approx 10 \times 10 \mu\text{m}^2$ . Values of  $OVC/(OVC + 1:1:2) < 0.09$  (cyan area) could not be resolved due to the background signal, but no OVCs were found in scanning (SEM) and transmission electron microscopy (TEM) for corresponding samples (not shown here).

Obviously, the OVC surface fraction decreases toward stoichiometric composition until eventually no OVCs can be measured for  $[I]/[III] > 0.97$ . For larger  $[I]/[III]$  values, the I-rich  $\text{Ag}_9\text{GaSe}_6$  phase starts to segregate,<sup>[28,43]</sup> possibly accompanied by a minor fraction of  $(\text{Ag}_y\text{Cu}_{1-y})_{2-x}\text{Se}$ . It is unclear if for common absorber deposition routines, a phase-pure 1:1:2 chalcopyrite film can be formed at perfect integral stoichiometry or if minor OVC and  $\text{Ag}_9\text{GaSe}_6$  segregations coexist. The corresponding data points for samples with  $AAC = 0.80$  and  $GGI = 0.85$  (majority of samples from the study by Keller et al.<sup>[28]</sup>) are added as well (gray dots). As intended, the OVC fraction in off-stoichiometric ACIGS ( $[I]/[III] < 0.9$ ) could be significantly reduced by decreasing the Ag and Ga content in this study. To highlight the trend, the OVC surface fraction for a CIGS sample with no Ga at the front is also added (taken from the study by Keller et al.<sup>[42]</sup>), exhibiting a further substantial reduction in OVC formation. This again confirms a narrowing of the 1:1:2 chalcopyrite single-phase region toward the ternary  $\text{AgGaSe}_2$  compound. The corresponding Raman spectra for the samples with different compositions, but with constant  $[I]/[III] = 0.82$ , are shown in **Figure 2b**. The peak positions of the OVC and 1:1:2 phases ( $A_1$  modes), which shift with composition, are highlighted.

In our previous work, we found that for values of  $OVC/(OVC + 1:1:2) > 0.4$ , as measured for  $[I]/[III] < 0.85$ , for the samples with  $AAC = 0.80$  and  $GGI = 0.85$ , large OVC patches formed also at the back contact. This observation correlated with a kink in  $I-V$  and corresponding FF losses.<sup>[28]</sup> Due to the larger

tolerance to off-stoichiometry for ACIGS with  $AAC \approx 0.60$  and  $GGI \approx 0.72$ , these OVCs (formed during the first stage of absorber processing) can be consumed during the second stage. Thus, the samples in this study do not show OVCs at the back contact. Consequently, a distortion in  $I-V$  characteristics is not observed, as will be shown later.

This feature is clearly shown in **Figure S2**, Supporting Information, which compares the in-depth OVC distribution for the samples indicated by small arrows in **Figure 2a** via TEM analysis supported by electron-dispersive X-ray spectroscopy (EDS). **Figure S2**, Supporting Information, further shows that a one-stage process leads to a rather random distribution of OVCs in the absorber.

## 2.2. Effect of Composition and Stoichiometry on Device Performance

The solar cell parameters for the best solar cells of each sample are shown as a function of absorber composition in **Figure 3**. The exact composition of the individual samples is indicated by a black dot (spanning the contour plot). No clear trend in  $V_{OC}$  is observed, showing values of 840–880 mV for the majority of samples. As a tendency, FF and  $J_{SC}$  (determined from external quantum efficiency [EQE] measurements for each sample) increase with decreasing Ga content. The latter can be easily explained by the reduction in bandgap with lower GGI. Overall, this leads to higher efficiencies for  $GGI < 0.72$ . No significant effect of the Ag content is found in the investigated compositional range. This may not be surprising, as all samples likely have a positive CBO (compare **Figure 1**), and  $E_g$  is not strongly affected for  $AAC < 0.7$ .<sup>[24,44]</sup>

It is obvious that for some samples the parameters change very abruptly (discontinuities in the contour plot), for example, showing a sudden decrease or increase in  $V_{OC}$ . This indicates that the absorber composition is not the only paramount criterion determining the cell characteristics.

**Figure 4** shows again the results from  $I-V$  characterization but this time as a function of stoichiometry. It is confirmed that the Ag content, displayed for each sample by the color code, does not have a significant effect. While FF and efficiency do not show

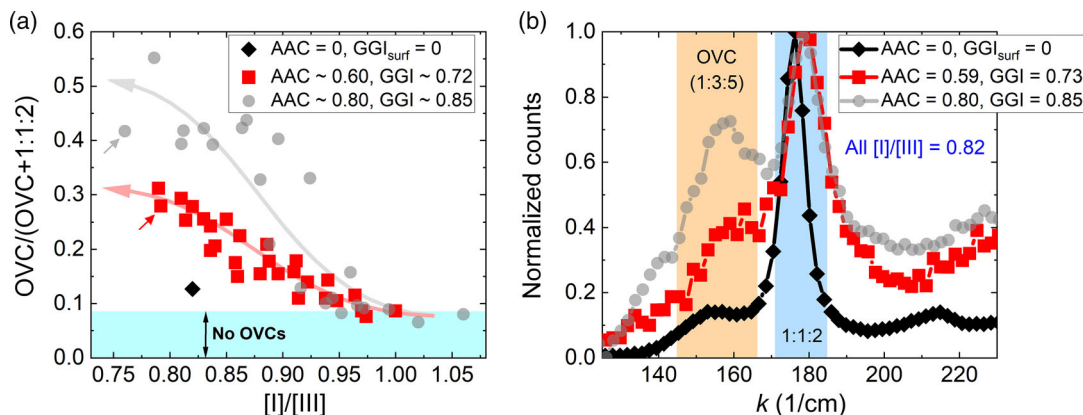


**Figure 2.** a) Normalized OVC peak intensities versus integral cation ratio for samples with different GGI and AAC values, as extracted from Raman measurements. b) Corresponding, exemplary Raman spectra on samples with constant  $[I]/[III] = 0.82$  and different compositions. Probing depth is  $\approx 200$  nm in all cases.



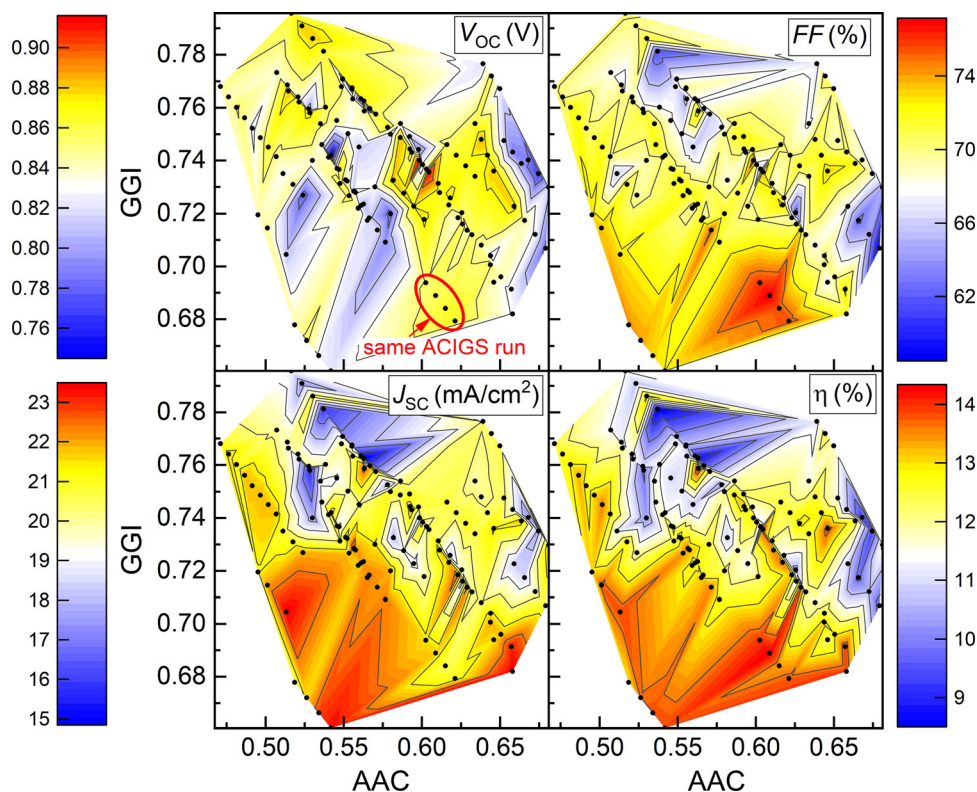


**Figure 3.** Solar cell parameters as a function of GGI and AAC, as extracted from  $I$ – $V$  analysis. Only the best cell values are shown and the dots (i.e., data points) show the actual sample compositions, which create the contour plot. The ellipse highlights four exemplarily samples/data points from the same ACIGS deposition run.

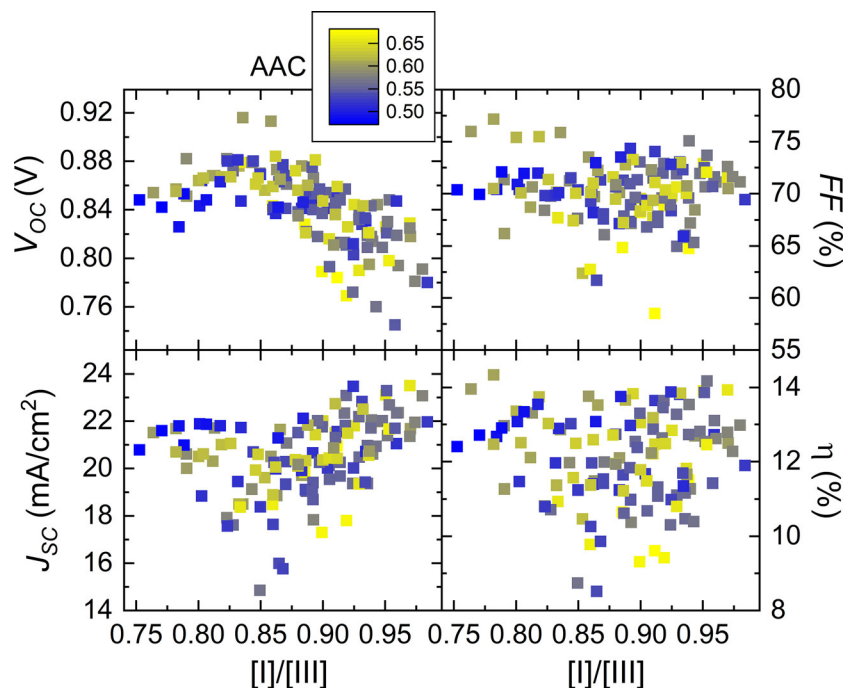


**Figure 4.** Solar cell parameters (best cells) as a function of cation ratio, extracted from  $I$ – $V$  analysis. The color code represents the corresponding AAC values.

a strong correlation with  $[I]/[III]$ , the stoichiometry obviously has an impact on  $V_{OC}$  and  $J_{SC}$ . More precisely,  $V_{OC}$  decreases and  $J_{SC}$  increases for  $[I]/[III] > 0.90$ . Samples with  $[I]/[III] < 0.90$  show  $\approx 100$  mV higher  $V_{OC}$  as compared with close-stoichiometric samples. For a very large off-stoichiometry,  $V_{OC}$  seems to decrease again slightly.

The opposing trend in  $J_{SC}$  is not as clear as for  $V_{OC}$ , as the effect of bandgap/compositional variations among the samples is more pronounced for  $J_{SC}$ . However, for almost all sample sets from individual absorber runs (i.e., similar  $E_g$ ), an increasing  $J_{SC}$  with increasing  $[I]/[III]$  value was observed.

To separate the effect of the bandgap energy from the impact of the stoichiometry,  $E_g$  was calculated for each sample from its respective composition (formula can be found here<sup>[24]</sup>). The resulting values are in very good agreement with the ones extracted from the respective EQE measurements (following a method presented in the study by Hages et al.<sup>[45]</sup>), which is an indication that only a very moderate GGI depth grading was implemented (compare Figure S3a,b, Supporting Information).

**Figure 5** shows the solar cell parameters as a function of  $E_g$ , where the color code displays the  $[I]/[III]$  value. The dashed gray lines show the percentage of the theoretical maximum values  $J_{SC,SQ}$  and  $V_{OC,SQ}$  for a given bandgap, according to Shockley–Queisser.<sup>[3]</sup> It is evident that the stoichiometry has a larger impact on  $V_{OC}$  than the bandgap, at least in the investigated compositional window. For sufficiently off-stoichiometric

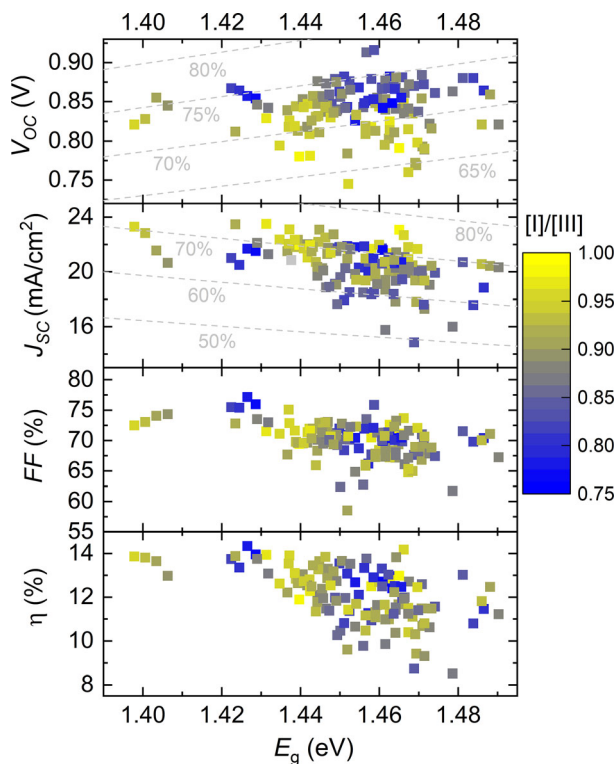


**Figure 5.** Solar cell parameters (best cells) as a function of bandgap energy, extracted from  $I$ – $V$  analysis. The color code represents the corresponding cation ratio and the dashed gray lines illustrate  $E_g$  values with constant percentage of the maximum possible  $J_{SC}$  and  $V_{OC}$  values, respectively.

absorbers ( $[I]/[III] < 0.9$ ), values of  $V_{OC} \approx 0.75 \cdot V_{OC,SQ}$  are possible for all compositions and bandgaps. The highest value of  $V_{OC} = 916$  mV  $= 0.78 \cdot V_{OC,SQ}$  is reached for AAC = 0.60, GGI = 0.74, and  $[I]/[III] = 0.83$  with  $E_g = 1.46$  eV. For more information about this sample, see Figure S3, Supporting Information. This is, to the best of our knowledge, the highest  $V_{OC}$  reported for a CdS-buffered chalcogenide solar cell at this bandgap energy (see Figure S4, Supporting Information). However, the  $V_{OC}$  loss is still greater than those for the best low-gap chalcopyrite solar cells ( $V_{OC} \approx 0.89 \cdot V_{OC,SQ}$ <sup>[2,42,46]</sup>). It is therefore suggested that the bulk properties are still inferior for wide-gap absorbers and that Ag alloying does not lead to a significant improvement in carrier lifetime. Unfortunately, the samples with the highest  $V_{OC}$  most often show low  $J_{SC}$  values, mainly triggered by the stoichiometry and not the composition.

As a general trend, FF decreases for  $E_g > 1.42$  eV. The bandgap increase can be mainly attributed to the increasing GGI and is not strongly affected by AAC. A possible reason for a decreasing FF may be that the photocurrent density ( $J_{PH}$ ) becomes more voltage dependent with increasing GGI. This would indicate a decrease in diffusion length ( $L_n$ ) with higher Ga content, which is in line with previous findings,<sup>[47]</sup> and again suggests that the bulk properties limit the device performance. However, other factors explaining the FF trend cannot be excluded, as will become clearer in the next section.

The anticorrelation in  $V_{OC}$  and  $J_{SC}$  results in a rather constant  $V_{OC} \times J_{SC}$  product for all samples, leaving the FF to define the trend in efficiency. Efficiencies of  $\approx 14\%$  (all without antireflection coating [ARC]) are reached for bandgap values up to  $E_g = 1.47$  eV, but the spread in  $\eta$  significantly increases with increasing bandgap. The opposing impact of stoichiometry on  $V_{OC}$  and  $J_{SC}$  makes the efficiency rather independent of the  $[I]/[III]$  value (as well as the AAC).

**Figure 6** shows the clear anticorrelation between  $V_{OC}$  and  $J_{SC}$  with varying cation ratios, again highlighting that the stoichiometry is the main factor defining the device parameters. Interestingly, for very low  $[I]/[III]$  values  $< 0.8$  (dark blue data points), the trend seems to be reversed again ( $J_{SC}$  increasing and  $V_{OC}$  decreasing). This observation is further discussed in

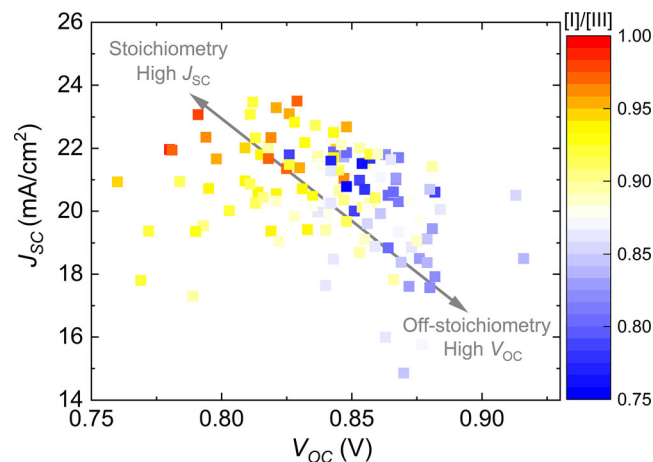


**Figure 6.** Correlation of  $J_{SC}$  and  $V_{OC}$  values of all samples (best cells). The color code represents the corresponding  $[I]/[III]$  values.

the next paragraph. To track down the origin of the  $J_{SC}$  loss for off-stoichiometric samples, a closer look on the corresponding EQE spectra, shown in Figure 7a, is reasonable.

To estimate the optical losses (except parasitic absorption in the buffer), the total reflectance ( $R_{cell}$ ) was measured on the completed device and the transmittance of the absorber layer ( $T_{abs}$ ) was measured on a bare ACIGS film on glass. Both samples have very similar composition of GGI  $\approx 0.74$  and AAC  $\approx 0.60$ . The discontinuity in  $T_{abs}$  at  $\lambda > 850$  nm originates from a sudden increase in reflection, because the bandgap energy of the absorber is reached and photons reflected at the ACIGS/glass interface can exit the front surface again. In addition, the parasitic absorption in the window layer ( $A_{win}$ ) was measured on a ZnO:Al/i-ZnO/glass sample. This allows approximating the maximum possible EQE (without internal collection losses) by the red dashed line in Figure 7a.

It is evident that the close-stoichiometric samples ( $0.95 < [I]/[III] < 0.98$ ) show almost perfect collection. The few samples with  $[I]/[III] \geq 0.98$  were excluded in Figure 7a to avoid confusion by interfering trends. Such (possibly over-) stoichiometric solar cells exhibit a wavelength-independent reduction in EQE that increases further with higher  $[I]/[III]$  values. Figure 7b shows this trend exemplarily for samples from two consecutive absorber runs with the same composition of GGI = 0.69, AAC = 0.65, and  $[I]/[III]$  values ranging from 0.89 to 1.00. The continuous and constant reduction in EQE for  $[I]/[III] \geq 0.98$  is likely caused by parasitic absorption in defect-rich  $Ag_9GaSe_6$  ( $E_g \approx 0.6$  eV), which forms for ACIGS with high Ag concentrations, instead of the binary and highly conductive  $(Ag_yCu_{1-y})_{2-x}Se$  phase commonly observed for low- or no-Ag-containing absorbers.<sup>[28,37,43]</sup>

For I-deficient samples, a long-wavelength reduction in EQE is observed that becomes more pronounced with decreasing  $[I]/[III]$  value. However, very low  $[I]/[III]$  values  $< 0.8$  seem to produce more squared spectra again. This trend was measured for the vast majority of samples stemming from the same absorber run, that is, highest  $J_{SC}$  for absorber closest to 1:1:2 stoichiometry. As large differences in absorption can be excluded, the EQE results reveal that the collection efficiency deeper in the absorber

is lower for off-stoichiometric samples. This can be either explained by a reduced diffusion length or a narrowed space-charge region (SCR). The origin of the collection losses and the corresponding increase in  $V_{OC}$  is elucidated in the next section.

### 2.3. Origin of $V_{OC}$ – $J_{SC}$ Anticorrelation with Varying Stoichiometry

To understand the impact of the stoichiometry on the device characteristics (i.e.,  $V_{OC}$ – $J_{SC}$  anticorrelation), this section focuses on four samples from a single absorber run with a composition of AAC = 0.53, GGI = 0.66, and a spread in stoichiometry of  $[I]/[III] = 0.89$ –0.95. These specific samples are exemplary for the majority of sample groups stemming from the same absorber deposition, exhibiting exactly the same trends.

Figure 8a shows the dark and light  $I$ – $V$  curves for the four samples with different  $[I]/[III]$  values. The sample closest to stoichiometric composition shows the highest  $J_{SC}$ , whereas the one most I deficient has the highest  $V_{OC}$ . The solar cells exhibit a similar, moderate crossover at  $V > 0.85$  V and show no  $I$ – $V$  distortion (kink), which holds for all other samples in this study. As shown in Figure 8a, the photocurrent is less voltage dependent (lower slope at  $V = 0$  V) for the close-stoichiometric solar cell as compared with the other samples. An appropriate way to investigate the extent of voltage-dependent collection is to determine the external collection efficiency  $\eta_C$  ( $J_{PH}(V) = J_{SC} \cdot \eta_C(V)$ ). Assuming that the diode current does not change under illumination and that  $\eta_C$  is independent of illumination intensity,  $\eta_C$  can be determined from the dark and light  $I$ – $V$  measurements:<sup>[48]</sup>

$$\eta_C(V) = \frac{J_{dark}(V) - J_{light}(V)}{J_{SC}} \quad (1)$$

The derived external collection efficiencies are shown in Figure 8b. Obviously, the close-stoichiometric sample suffers the least from incomplete collection. Only  $\approx 1\%$  is gained in  $J_{PH}$  at  $V = -0.4$  V for  $[I]/[III] = 0.95$ , whereas for lower  $[I]/[III]$

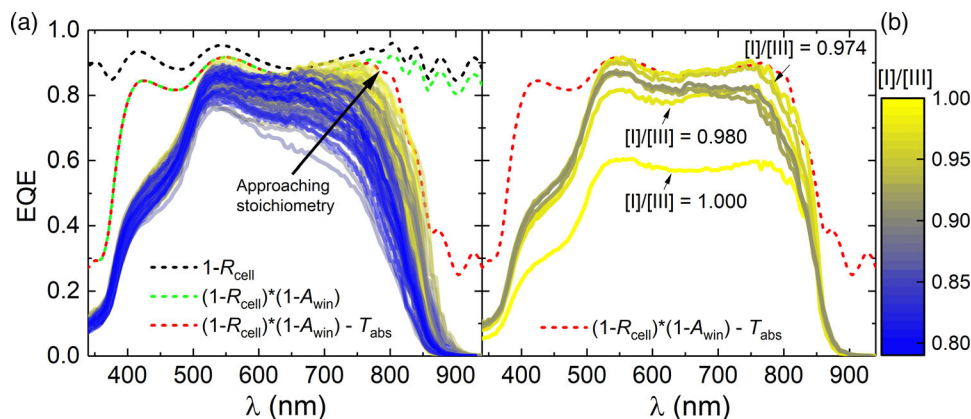


**Figure 7.** a) EQE spectra of all samples (best cells), excluding the ones with  $[I]/[III] \geq 0.98$ . The color represents the corresponding  $[I]/[III]$  values (same color bar for (a) and (b)). Lines are semitransparent for better illustration. Reflection (dashed black line) plus parasitic absorption losses in the TCO (green dashed line) and finally with included transmission losses (red dashed line) are added as an approximation of the maximum possible EQE. b) Exemplary EQE curves of samples from two consecutive absorber runs with the same composition of GGI = 0.69, AAC = 0.65, and  $[I]/[III] = 0.89$ –1.00.

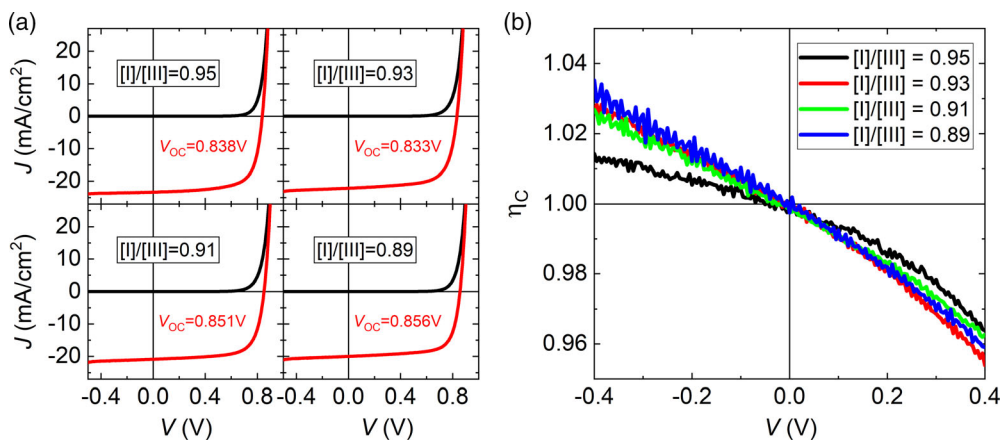


**Figure 8.** a) Exemplary  $I$ – $V$  characteristics (dark and light) of four samples from the same absorber deposition run with AAC = 0.53, GGI = 0.66, and [I]/[III] ranging from 0.89 to 0.95. b) Corresponding external collection efficiencies of the same samples.

values, the relative  $J_{PH}$  gain is a factor of three higher ( $\approx 3\%$ ) at this voltage. The most likely explanation for this observation is the expansion/shrinking of the SCR upon negative/positive voltage bias, if perfect collection is assumed in the SCR. However, changing heights of a potential charge transport barrier (e.g., at the OVC/CdS interface) or different degrees of interface recombination (e.g., by different fractions of OVC patches) may lead to similar  $\eta_c(V)$  trends.<sup>[48]</sup>

Overall, the detailed  $I$ – $V$  analysis is in line with the trends in EQE, shown in Figure 7, and again suggests that stoichiometric samples either contain a wider SCR or have a higher  $L_n$  (i.e., improved bulk properties).

The corresponding EQE spectra of the four samples are shown in Figure 9a. As for most of the solar cells in this study, the long-wavelength loss increases with decreasing [I]/[III] value. To study if the differences in  $\eta_c(V)$  arise from depth-dependent changes in collection efficiency (expected for varying SCR width and/or  $L_n$ ) or rather stem from altered interface recombination or transport barriers, each sample was measured at a negative ( $-0.5$  V) and positive ( $+0.5$  V) voltage bias, see Figure 9b–e. It is evident that the voltage bias affects the collection efficiency in different ways, depending on the wavelength region and absorber stoichiometry. To emphasize the relative effect of the different biases, the corresponding  $EQE_{bias}/EQE_{no\ bias}$  ratios are shown in Figure 9f. The wavelength region  $\lambda > 850$  nm is cut out, as the values become too noisy. Notably, the largest effect of the voltage bias is observed for  $\lambda < 520$  nm, which corresponds to the bandgap energy of the CdS layer. This indicates that the gain/loss in this wavelength region is related to photoinduced changes in the buffer layer, which were reported earlier.<sup>[49–52]</sup> Possible explanations may be that with increasing voltage bias, the absorption in CdS leads to 1) an increased interface recombination or 2) a decreasing carrier collection in the buffer itself. However, this feature remains speculative at this point and even an artifact of the applied lock-in technique cannot be excluded as its origin.<sup>[51]</sup>

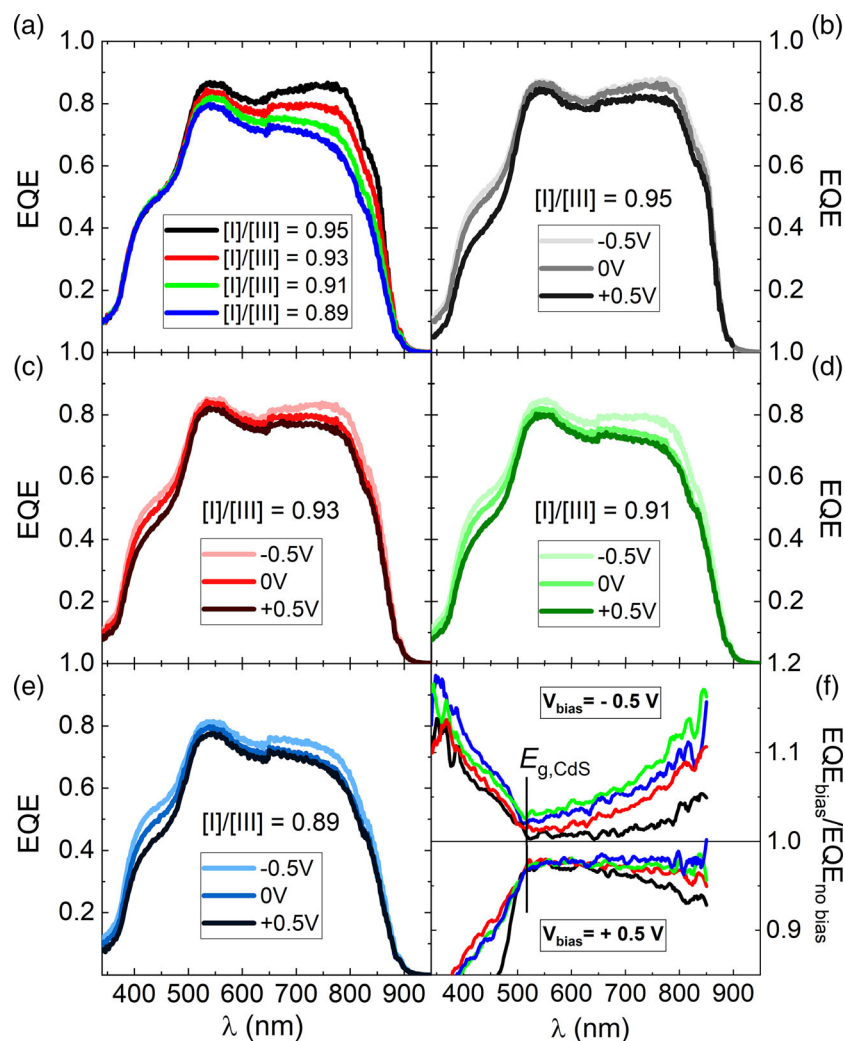
For  $\lambda > 520$  nm, the effect of the voltage bias strongly depends on the [I]/[III] value. The negative voltage bias has the smallest effect for the close-stoichiometric sample. Here, a slight gain in

EQE is only measured for  $\lambda > 750$  nm, suggesting a very high  $L_n$  or wide SCR. In contrast, the off-stoichiometric samples exhibit a clear improvement in carrier collection when expanding the SCR. The EQE gain for these cells is continuously increasing for  $\lambda > 520$  nm, suggesting a smaller  $L_n$  or narrower SCR for the more I-deficient samples. A positive voltage bias has a smaller effect on the EQE curves. In this case, all samples exhibit a similar and less wavelength-dependent reduction in carrier collection. Only the close-stoichiometric sample shows a clear wavelength-dependent loss in EQE, similar to the gain observed at negative bias. At this point it is not understood why the positive bias leads to less relative losses with decreasing [I]/[III] value.

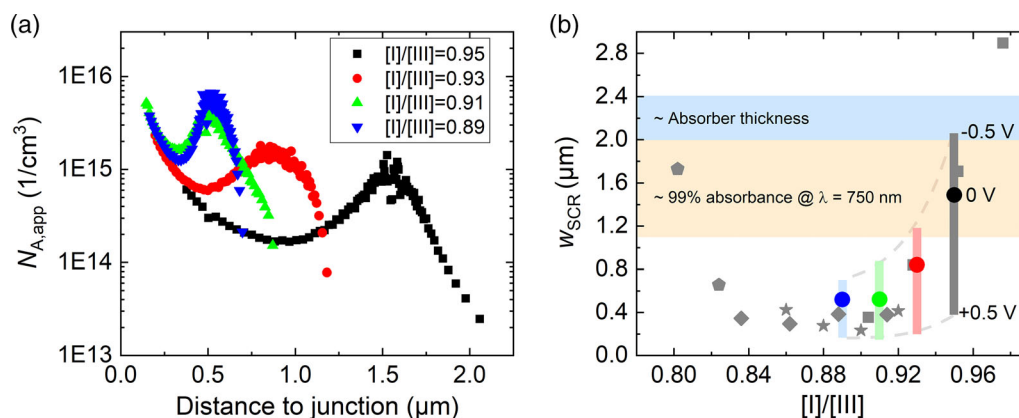
To identify if the observed collection losses for off-stoichiometric samples arise from a reduced  $L_n$  or a narrower SCR (or both), capacitance–voltage ( $C$ – $V$ ) measurements were carried out on the four exemplary samples. The resulting doping profiles, measured from  $V = -0.5$  V to  $+0.5$  V, are shown in Figure 10a. Obviously, the apparent doping density  $N_{A,app}$  decreases toward stoichiometric ACIGS composition, dropping from  $N_{A,app} \approx 7 \times 10^{15} \text{ cm}^{-3}$  for [I]/[III] = 0.89 to  $N_{A,app} \approx 1 \times 10^{15} \text{ cm}^{-3}$  for [I]/[III] = 0.95. It should be noted that the apparently similar, very high doping densities at small distances from the junction (high positive voltages) may be an artifact from charge injection, resulting in an additional injection capacitance, as recently reported.<sup>[53]</sup> A peculiarity observed for all samples is that the doping level seemingly shows a plateau (or broad peak) around  $w_{SCR}$  at  $V = 0$  V. All corresponding Mott–Schottky plots, shown in Figure S5, Supporting Information, exhibit a strong deviation from linearity (i.e., variation in extracted doping density) for voltages of  $V < -0.3$  V and  $V > +0.2$  V. This feature is not understood at this point and requires further investigation in the future.

Figure 10b shows the corresponding SCR widths ( $w_{SCR}$ ) at  $V = 0$  V as a function of the corresponding [I]/[III] value (same color assignment as in (a)). The range of absorber thicknesses used in this study is indicated, too. As a result of the very low doping, the close-stoichiometric absorber is almost fully depleted ( $w_{SCR} \approx 1.5 \mu\text{m}$ ), whereas  $w_{SCR}$  is reduced to about 840 nm for [I]/[III] = 0.93 and saturates at  $w_{SCR} \approx 520$  nm for lower





**Figure 9.** a) Exemplary EQE curves of four samples from the same absorber deposition run with AAC = 0.53, GGI = 0.66, and [I]/[III] ranging from 0.89 to 0.95. b–e) Corresponding EQE curves under negative and positive voltage bias. f) Corresponding relative effect of different voltage biases (same color assignment as in (a)).



**Figure 10.** a) Exemplary apparent doping profiles of four samples from the same absorber deposition run with AAC = 0.53, GGI = 0.66, and [I]/[III] ranging from 0.89 to 0.95. b) Corresponding extensions of the SCR at  $V = -0.5$  V, 0, and  $+0.5$  V (same color assignment as in (a)). The additional data points in gray stem from solar cells from four different absorber runs (corresponding to different symbols).



[I]/[III] values. To confirm this trend, 14 additional samples from four different absorber runs were measured as well (gray data points). The results are consistent, emphasizing that the doping density clearly decreases toward 1:1:2 stoichiometry for [I]/[III] > 0.92. However, for a very pronounced off-stoichiometry ([I]/[III] ≤ 0.82), the doping apparently decreases again. A sample with [I]/[III] = 0.974 showed a  $w_{\text{SCR}}$  larger than the absorber depth, indicating that the dielectric constant ( $\epsilon_r = 12$ ) was slightly overestimated in the analysis.

The increasing width of the SCR correlates with the increased carrier collection observed for samples approaching stoichiometric composition. Obviously, full absorber depletion is necessary for perfect collection. This strongly indicates a very low diffusion length in wide-gap ACIGS and suggests that carrier collection is almost negligible in the quasineutral region (QNR).

To link the changes in SCR width with the effect of the bias in EQE (Figure 9), the generation profile has to be estimated. This was done by approximating a 99% light attenuation for  $\lambda = 750$  nm, that is, a wavelength for which a clear collection loss is measured for off-stoichiometric samples, from absorption data reported for CIGS with a similar GGI ( $\alpha(750 \text{ nm}) \approx 2 \times 10^6 - 5 \times 10^6 \text{ 1/m}$ ).<sup>[54,55]</sup> The resulting absorption depth (highlighted in Figure 10(b)) is in good agreement with the optical transmission of  $T_{\text{abs}, \lambda = 750 \text{ nm}} = 0.3\%$ , as measured on a bare, 2  $\mu\text{m}$ -thick absorber sample on glass (see  $T_{\text{abs}}$  in Figure 7). The change in  $w_{\text{SCR}}$  when sweeping the voltage from  $-0.5$  to  $+0.5$  V (same as bias in EQE in Figure 9) is indicated by a bar for each sample in Figure 10b.

In case of the close-stoichiometric sample with [I]/[III] = 0.95,  $w_{\text{SCR}}$  lies at a depth of insignificant carrier generation. Thus, a further expansion by a negative bias does not increase the carrier collection notably, which is in line with the EQE results. At  $V = +0.5$  V,  $w_{\text{SCR}}$  reduces to  $\approx 400$  nm that should result in a considerable reduction in long-wavelength EQE, as shown in Figure 9b. However, if collection is negligible in the QNR, the EQE at  $V = +0.5$  V should fall below the nonbiased EQE of the sample with [I]/[III] = 0.93 that shows a  $w_{\text{SCR}}$  of about 840 nm. Due to the mentioned potential impact of an injection capacitance,<sup>[53]</sup>  $w_{\text{SCR}}$  may be largely overestimated at positive bias, which could explain this discrepancy. For the samples with lower [I]/[III] values,  $w_{\text{SCR}}$  is located at a depth of significant electron generation. Consequently, the negative voltage bias has a stronger effect on carrier collection, in agreement with Figure 9c–f. At this point it is not clear though, why the samples with [I]/[III] ≤ 0.93 did not show a more pronounced EQE loss at  $V = +0.5$  V, as the  $C-V$  measurements suggest a substantially narrowed SCR width in a region of very high electron generation.

It can be summarized that the low  $J_{\text{SC}}$  values of the off-stoichiometric solar cells are likely caused by a very low  $L_n$ . The corresponding collection loss can only be avoided by depleting the absorber, as it is found for close-stoichiometric absorbers. This is in line with earlier studies, proving that voltage-dependent carrier collection becomes more dominant with increasing GGI in CIGS solar cells.<sup>[47]</sup> Assuming that the low  $L_n$  is caused by energetically deep  $\text{Ga}_1$  defects,<sup>[8–11]</sup> it may be speculated that  $\text{Ga}_{\text{Ag}}$  in ACIGS is similarly abundant and/or detrimental (i.e., deep) as  $\text{Ga}_{\text{Cu}}$ .

The low doping required for a high  $J_{\text{SC}}$  results in a reduction of the built-in potential, which potentially reduces  $V_{\text{OC}}$ .

Assuming dominant recombination in the SCR at  $V \approx V_{\text{OC}}$ , the observed reduction in doping density by a factor of  $\approx 7$  leads to a  $V_{\text{OC}}$  loss of  $\approx 25$ – $50$  mV (depending on the ideality factor),<sup>[56]</sup> which is in the range measured in this study. That may also explain why the  $V_{\text{OC}}$  values decrease again for very low [I]/[III], where the doping apparently decreases again. Overall, it appears likely that changes in doping concentration are responsible for the anticorrelation in  $V_{\text{OC}}$  and  $J_{\text{SC}}$  observed for varying ACIGS stoichiometry.

The revealed trends in ACIGS doping are in contrast to other studies on  $\text{CuInSe}_2$  and  $\text{CuGaSe}_2$ , which often show higher hole densities with increasing [I]/[III] values,<sup>[57–59]</sup> especially when crossing the border from Cu-poor to Cu-rich composition.<sup>[59,60]</sup> A high degree of compensation is assumed for I-poor CIGS material,<sup>[61]</sup> by forming large quantities of either isolated shallow  $\text{In}_{\text{Cu}}$  donor and  $\text{V}_{\text{Cu}}$  acceptor defects<sup>[9]</sup> or  $(2\text{V}_{\text{Cu}}^- + \text{In}_{\text{Cu}}^{2+})$  complexes.<sup>[62]</sup> The very low doping found in this study may indicate that Ag alloying increases the degree of compensation for [I]/[III] > 0.92. An alternative explanation could be the possibility of approaching the stoichiometric point closer (i.e., low  $\text{V}_{\text{Cu}}$  density  $\rightarrow$  low doping) for ACIGS without the need to selectively etch any detrimental  $\text{Cu}_{2-x}\text{Se}$  phase, as the rather resistive  $\text{Ag}_3\text{GaSe}_6$  compound forms instead. It was further found that the presence of Na in the absorber bulk plays a key role in the doping mechanism, usually leading to increased majority carrier densities.<sup>[63–67]</sup> As the solubility limit of Na in the ACIGS lattice (on  $\text{V}_1$ ) increases with the Ag content,<sup>[68]</sup> it may be speculated that Na saturation is not reached during absorber processing, resulting in lower doping. Further studies are needed to reveal the exact relationship between doping, stoichiometry and Na distribution.

## 2.4. General Considerations Regarding Wide-Gap ACIGS

This section shall summarize the effects of stoichiometry on the three-stage-processed wide-gap ACIGS (AAC and GGI > 0.5) with respect to the resulting phase distribution and solar cell characteristics. Figure 11 sketches the corresponding trends found in this study or reported in earlier works.<sup>[24,28–30,43]</sup> The [I]/[III] range in which the transition between the different features occurs (e.g., OVCs at the back contact or not) decreases with increasing Ag and Ga content, due to the narrowing of the 1:1:2 single-phase region.

For very I-deficient absorbers (A), large OVC patches form at the back and front contact (see also Figure 1). Their presence at the back correlates with low FF values, resulting from an evolving transport barrier. It was speculated that the strong Na accumulation in the OVCs leads to a reduced alkali concentration at the ACIGS/ $\text{MoSe}_2$  interface, thereby creating a Schottky contact. In addition, a long-term redistribution of Na in the absorber (1:1:2 and OVCs) and at its interfaces was suggested as the root cause of further degradation.<sup>[28]</sup> The samples in this study have low-enough Ag and Ga contents to prevent OVC formation at the back contact even for the lowest [I]/[III] value of 0.75. The fact that not a single I-deficient solar cell showed a kink in  $I-V$  supports the hypothesis stated above.

When increasing the [I]/[III] value (B), the OVCs at the back contact are consumed during the second stage of ACIGS deposition and only OVCs at the front remain. A high FF and  $V_{\text{OC}}$  is

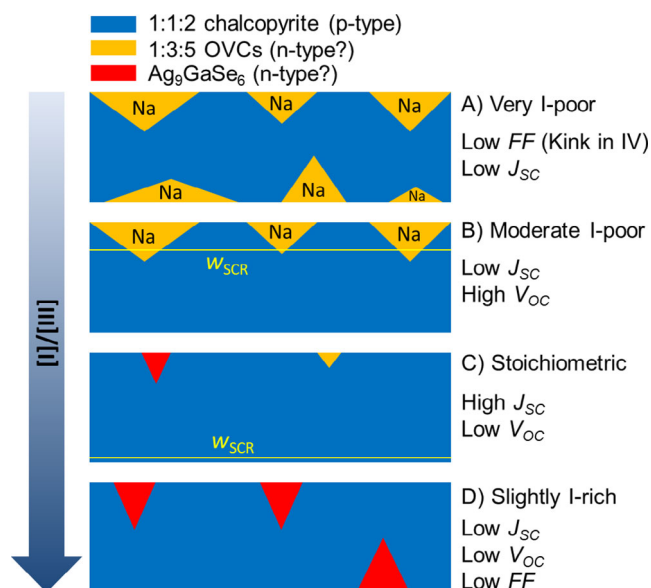


**Figure 11.** Sketched phase distribution, in the three-stage processed, wide-gap (GGI and AAC > 0.5) ACIGS absorbers, depending on the integral  $[I]/[III]$  ratio.

accompanied by a rather low  $J_{SC}$ . In our previous study, we assigned the corresponding collection loss to the OVCs at the surface.<sup>[28]</sup> However, this work rather suggests that the SCR is too narrow for moderately I-deficient absorbers to ensure adequate carrier collection, as wide-gap ACIGS films obviously suffer from a very low  $L_n$ . Still, it would be surprising if the OVCs at the front are electronically inactive and entirely irrelevant for device performance. The OVC patches exhibit a larger bandgap ( $\Delta E_g \approx 0.2\text{--}0.3\text{ eV}$ ) as compared with the surrounding 1:1:2 phase.<sup>[28,43,69–74]</sup> Although they do not cover the whole surface, a somewhat beneficial effect on  $V_{OC}$  cannot be excluded just by the larger  $E_g$ . In addition, a very pronounced CBO (“spike” > 0.4 eV) at the OVC/1:1:2 and OVC/CdS interfaces is expected for the measured absorber and OVC compositions.<sup>[17,28,33–36]</sup> Such a large conduction band discontinuity should result in significant collection losses of electrons generated inside (or diffused into) the OVCs.<sup>[23]</sup> However, an associated kink in EQE at the estimated OVC bandgap energy ( $\lambda \approx 750\text{ nm}$ ) was not observed, which implies that the sheer presence of the OVCs does not deteriorate the collection efficiency (in contrast to what we claimed earlier<sup>[28]</sup>). In the future, we plan for electron beam-induced current measurements on the solar cell cross sections to confirm this hypothesis.

For (close-) stoichiometric absorbers (C), (almost) full depletion is measured, resulting in a perfect carrier collection, despite the low diffusion length. However, the reduced doping density causes a substantial drop in  $V_{OC}$ . Very little to no OVC fraction is assumed at the stoichiometric point. It is unclear though if a phase-pure 1:1:2 chalcopyrite film can be formed in a common three-stage process or if minor OVCs and  $\text{Ag}_9\text{GaSe}_6$  segregations coexist.

Finally, all solar cell parameters start to deteriorate for I-rich compositions (D, in this study for  $[I]/[III] \geq 0.98$ , presumably due to a slight offset in calibration), as a result of the substantial

formation of  $\text{Ag}_9\text{GaSe}_6$ . This phase is not very conductive but has a low  $E_g$  and is likely defect rich.<sup>[43]</sup>

Summarizing all findings, it can be concluded that Ag alloying reduces recombination at the buffer interface in chalcopyrite solar cells with  $\text{GGI} > 0.5$ .<sup>[24]</sup> This allows producing such low  $V_{OC}$  deficits with CdS as only possible for pure CIGS when using alternative buffers (see Figure S4, Supporting Information). However, even after eliminating interface recombination, the  $V_{OC}$  of ACIGS devices is still limited to values  $< 0.8 \cdot V_{OC, SQ}$ , as observed for all chalcopyrite solar cells with  $\text{GGI} > 0.5$  (see again Figure S4, Supporting Information). This can be attributed to poor bulk properties. A very low diffusion length was also confirmed in this study, being responsible for the low carrier collection for only partially depleted absorbers. As mentioned, the “electron killer” is likely the deep  $\text{Ga}_I$  defect. Its potential absence or mitigation in low-gap absorbers allows for  $V_{OC}$  values approaching  $0.9 \cdot V_{OC, SQ}$ .<sup>[2,46,75]</sup> Nevertheless, other factors like Cu-enriched grain boundaries<sup>[15]</sup> or a larger density of acceptor defects<sup>[12,13]</sup> may contribute to the  $V_{OC}$  loss at high GGI values as well.

Thus, the bottleneck for increasing the efficiency of wide-gap ACIGS solar cells is the low electron lifetime. In the case of low-gap CIGS, introduction of heavy alkali elements like K, Rb, or Cs led to significantly enhanced lifetimes.<sup>[76,77]</sup> Also for CIGS with  $\text{GGI} \geq 0.6$ , some authors report a longer lifetime after heavy alkali incorporation,<sup>[78]</sup> whereas others suggest a negligible effect.<sup>[79]</sup> Another way to increase the carrier collection without reducing the doping in ACIGS (by approaching stoichiometric composition) is the fine tuning of the Ga depth profile. Already, a moderate bandgap grading can lead to a substantial increase in effective diffusion length.<sup>[80]</sup> Thus, a continuous reduction in GGI from the back contact to the edge of the SCR is desirable to enhance the collection probability in the QNR. The GGI is rather constant in the upper half of the absorbers in this study (see Figure S3, Supporting Information), which motivates an optimization of the compositional profile. A first attempt to implement a more suitable GGI profile was done by extending the increased Ga evaporation rate into the second stage of absorber processing (Figure S6a, Supporting Information). As intended, a continuous GGI grading was achieved, which led to significantly reduced collection losses for a cell with a distinct I deficiency of  $[I]/[III] = 0.86$ . This sample exhibits an efficiency of  $\eta = 14.9\%$  ( $V_{OC} = 862\text{ mV}$ ,  $J_{SC} = 22.9\text{ mA cm}^{-2}$ ,  $\text{FF} = 75.5\%$ ) at a bandgap of 1.44 eV, better than all other cells processed in this study (see Figure S6b–d, Supporting Information).

Finally, although CdS is a mature and stable buffer layer, alternative materials like  $(\text{Zn}, \text{Sn})\text{O}$  are suggested for wide-gap chalcopyrite solar cells, as parasitic absorption in the buffer leads to increasing relative  $J_{SC}$  losses for larger  $E_g$ . In addition, alternative buffers with tunable electron affinity allow for a larger range of compositions resulting in a spike-like interface configuration.<sup>[24]</sup> A low-electron affinity buffer in combination with AAC values  $\leq 0.5$  may be favorable to exclude long-term degradation, accordingly.<sup>[28]</sup>

### 3. Conclusion

The effect of absorber stoichiometry in wide-gap ACIGS solar cells (AAC  $\approx 0.5\text{--}0.7$  and  $\text{GGI} \approx 0.7\text{--}0.8$ ) is revised. It is found

that the stoichiometry has a strong and opposing effect on  $J_{SC}$  and  $V_{OC}$ . With increasing  $[I]/[III]$  values  $> 0.9$ ,  $V_{OC}$  continuously decreases, whereas charge carrier collection and thus  $J_{SC}$  increases. Capacitance profiling identified a strong decrease in doping density toward stoichiometric ACIGS as the root cause for the anticorrelation in  $J_{SC}$  and  $V_{OC}$ . However, a possible contribution from OVCs at the front contact cannot be ruled out.

As only fully depleted stoichiometric samples show perfect carrier collection, a very low diffusion length can be assumed to be the bottleneck for wide-gap ACIGS solar cells. This implies that Ag alloying does not change the bulk recombination (e.g., via deep  $Ga_I$  defects) considerably. Finally, a solar cell with  $V_{OC} = 0.916$  V was achieved at  $E_g = 1.46$  eV, which is the highest value reported for this bandgap to date.

Possible ways forward are the 1) introduction of heavy alkali elements to increase the carrier lifetime, 2) optimization of the Ga profile to increase the “effective” diffusion length, and 3) application of alternative buffers to minimize parasitic absorption allowing for lower Ag contents without forming a negative CBO.

## 4. Experimental Section

**Solar Cell Processing:** Solar cells were processed as a stack of soda lime glass (SLG)/Mo/NaF/ACIGS/CdS/i-ZnO/ZnO:Al. The Mo back electrode was sputtered (DC) on the SLG substrates. In the next step, NaF (10–15 nm) was evaporated on top. No alkali diffusion barrier was used, so Na in-diffusion from the SLG was allowed. Subsequently, ACIGS films were grown via a three-stage (I poor  $\rightarrow$  I rich  $\rightarrow$  I poor) coevaporation process. The Ag/Cu evaporation rate ratio was kept constant at any time. To implement a back-surface field, a higher Ga and lower In rate were applied during the initial absorber growth. The deposition scheme is shown in Figure S6a, Supporting Information. All ACIGS films exhibited similar GGI depth profiles, akin to the one shown in Figure S3b, Supporting Information, and the thickness varied between 2.0 and 2.4  $\mu\text{m}$ . The maximum substrate temperature during the second and third stage was set to 550 °C. No alkali postdeposition treatment was applied. The absorber compositions from a total of 40 ACIGS depositions were  $AAC = 0.47\text{--}0.67$  and  $GGI = 0.66\text{--}0.79$  with a stoichiometry variation of  $0.75 \leq [I]/[III] \leq 1.00$ . Integral compositions were extracted from cross-calibrated X-ray fluorescence measurements on bare absorbers located at the outer positions of the deposition zone. Four samples with different (linearly interpolated)  $[I]/[III]$  values were extracted from each ACIGS deposition run. After absorber formation, a 50 nm-thick CdS buffer layer was grown by chemical bath deposition. The solar cell stacks were finalized by sputtering i-ZnO (70 nm) and ZnO:Al (150 nm; sheet resistance  $\approx 50 \Omega \text{ sq}^{-1}$ ) on top. No ARC was used for any of the cells in this study. Finally, all samples were sectioned into 14 solar cells ( $A = 0.05 \text{ cm}^2$ ) by mechanical scribing. A total of 139 samples was investigated (i.e., 21 I-rich samples were disregarded).

**Absorber Characterization and Optical Analysis:** The OVC phase fraction at the absorber surface was quantified by Raman spectroscopy (Renishaw inVia) using a laser with 532 nm excitation wavelength ( $\approx 200$  nm probing depth) at  $20\times$  magnification. Elemental depth profiles were measured by glow discharge optical emission spectroscopy in a Spectra Analytik GDA 750HR system. SEM analysis, utilizing a Zeiss Merlin instrument ( $V_{acc} = 5 \text{ kV}$ ), was used to investigate the solar cell cross sections. Scanning TEM on a FEI Titan Themis XFEI instrument assisted by EDS allowed identification of OVC patches and illustration of their distribution. The TEM lamellae were prepared via focused ion beam and subsequent liftoff. The transmission of a bare absorber film on glass, the reflection of a complete solar cell, and the absorption of the window layer stack were measured in a Perkin Elmer Lambda 900 spectrometer with an integrating sphere.

**Electro-Optical Characterization of Solar Cells:** Completed solar cells were characterized by EQE and  $I$ – $V$  measurements in home-built setups with a delay of 1–3 days after the absorber processing. The latter was conducted at  $T = 25^\circ\text{C}$  and under illumination by an ELH lamp. The light intensity during  $I$ – $V$  analysis was calibrated for each sample to match the  $J_{SC,EQE}$  value, as calculated from the EQE spectra for illumination with the AM1.5G spectrum.  $C$ – $V$  profiling was conducted from  $V = -0.5$  to  $0.5$  V at 50 kHz and an amplitude of 25 mV. A dielectric constant of  $\epsilon_r = 12$  was assumed for the ACIGS material in this study.

## Supporting Information

Supporting Information is available from the Wiley Online Library or from the author.

## Acknowledgements

This work was supported by the Swedish Foundation for Strategic Research (SSF) under the project number RMA15-0030 and by the Swedish Energy Agency under the project number P50992-1, Dnr 2020-009335. The authors also thank Dr. Olivier Donzel-Gargand for conducting the transmission electron microscopy analysis.

## Conflict of Interest

The authors declare no conflict of interest.

## Data Availability Statement

Research data are not shared.

## Keywords

(Ag,Cu)(In,Ga)Se<sub>2</sub>, Cu(In,Ga)Se<sub>2</sub>, ordered vacancy compounds, stoichiometry, wide-gap chalcopyrites

Received: June 9, 2021

Revised: June 28, 2021

Published online:

- [1] P. Jackson, R. Wuerz, D. Hariskos, E. Lotter, W. Witte, M. Powalla, *Phys. Status Solidi RRL*. **2016**, 586, 583.
- [2] M. Nakamura, K. Yamaguchi, Y. Kimoto, Y. Yasaki, T. Kato, H. Sugimoto, *IEEE J. Photovoltaics*. **2019**, 9, 1863.
- [3] W. Shockley, H. J. Queisser, *J. Appl. Phys.* **1961**, 32, 510.
- [4] A. S. Brown, M. A. Green, *Phys. E*. **2002**, 14, 96.
- [5] R. K. Kothandaraman, Y. Jiang, T. Feuer, A. N. Tiwari, F. Fu, *Small Methods*. **2020**, 4, 2000395.
- [6] S. Siebentritt, U. Rau, *Wide-Gap Chalcopyrites*, Springer-Verlag, Berlin Heidelberg **2006**.
- [7] M. A. Contreras, L. M. Mansfield, B. Egaas, J. Li, M. Romero, R. Noufi, E. Rudiger-Voigt, W. Mannstadt, *Prog. Photovolt. Res. Appl.* **2012**, 20, 843.
- [8] B. Huang, S. Chen, H. Deng, L. Wang, M. A. Contreras, R. Noufi, S.-H. Wei, *IEEE J. Photovoltaics*. **2014**, 4, 477.
- [9] J. Pohl, K. Albe, *Phys. Rev. B*. **2013**, 87, 245203.
- [10] C. Spindler, F. Babbe, M. H. Wolter, F. Ehre, K. Santosh, P. Hilgert, F. Werner, S. Siebentritt, *Phys. Rev. Mater.* **2019**, 3, 090302.
- [11] C. Spindler, D. Regesch, S. Siebentritt, *Appl. Phys. Lett.* **2016**, 109, 032105.

- [12] G. Hanna, A. Jasenek, U. Rau, H. W. Schock, *Thin Solid Films*. **2001**, 387, 71.
- [13] G. Hanna, A. Jasenek, U. Rau, H. W. Schock, *Phys. Status Solidi A*. **2000**, 179, R7.
- [14] M. Raghuwanshi, R. Wuerz, O. Cojocaru-Mirédin, *Adv. Funct. Mater.* **2020**, 30, 2001046.
- [15] M. Raghuwanshi, E. Cadel, P. Pareige, S. Duguay, F. Couzinie-Devy, L. Arzel, N. Barreau, *Appl. Phys. Lett.* **2014**, 105, 013902.
- [16] M. R. Balboul, H. W. Schock, S. A. Fayak, A. A. El-Aal, J. H. Werner, A. A. Ramadan, *Appl. Phys. A*. **2008**, 92, 557.
- [17] S.-H. Wei, A. Zunger, *J. Appl. Phys.* **1995**, 78, 3846.
- [18] M. Gloeckler, J. R. Sites, *Thin Solid Films*. **2005**, 480–481, 241.
- [19] M. Turcu, O. Pakma, U. Rau, *Appl. Phys. Lett.* **2002**, 80, 2598.
- [20] A. Jasenek, U. Rau, V. Nadenau, H. W. Schock, *J. Appl. Phys.* **2000**, 87, 594.
- [21] V. Nadenau, U. Rau, A. Jasenek, H. W. Schock, *J. Appl. Phys.* **2000**, 87, 584.
- [22] F. Larsson, N. S. Nilsson, J. Keller, C. Frisk, V. Kosyak, M. Edoff, T. Törndahl, *Prog. Photovolt. Res. Appl.* **2017**, 25, 755.
- [23] J. Lindahl, J. Keller, O. Donzel-Gargand, P. Szaniawski, M. Edoff, T. Törndahl, *Sol. Energy Mater. Sol. Cells*. **2016**, 144, 684.
- [24] J. Keller, K. V. Sopiha, O. Stolt, L. Stolt, C. Persson, J. J. S. Scragg, T. Törndahl, M. Edoff, *Prog. Photovolt. Res. Appl.* **2020**, 28, 237.
- [25] G. M. Hanket, J. H. Boyle, W. N. Shafarman, in *34th IEEE Photovolt. Spec. Conf.* **2009**, 001240.
- [26] T. Nakada, K. Yamada, R. Arai, H. Ishizaki, N. Yamada, *MRS Proc.* **2005**, 865, F11.1.
- [27] T. Umehara, F. Zulkifly, K. Nakada, A. Yamada, *Jpn. J. Appl. Phys.* **2017**, 56, 08MC09.
- [28] J. Keller, L. Stolt, K. V. Sopiha, J. K. Larsen, L. Riekehr, M. Edoff, *Sol. RRL*. **2020**, 4, 2000508.
- [29] H. Simchi, B. McCandless, W. Shafarman, K. Kim, J. Boyle, R. Birkmire, in *37th IEEE Photovolt. Spec. Conf.* **2011**, 000041.
- [30] J. H. Boyle, B. E. McCandless, G. M. Hanket, W. N. Shafarman, *Thin Solid Films*. **2011**, 519, 7292.
- [31] F. Pianezzi, P. Reinhard, A. Chirilă, B. Bissig, S. Nishiwaki, S. Buecheler, A. N. Tiwari, *Phys. Chem. Chem. Phys.* **2014**, 16, 8843.
- [32] J.-H. Yoon, J.-H. Kim, W. M. Kim, J.-K. Park, Y.-J. Baik, T.-Y. Seong, J. Jeong, *Prog. Photovolt. Res. Appl.* **2014**, 22, 90.
- [33] A. Sharan, F. P. Sabino, A. Janotti, N. Gaillard, T. Ogitsu, J. B. Varley, *J. Appl. Phys.* **2020**, 127, 065303.
- [34] S. B. Zhang, S.-H. Wei, A. Zunger, H. Katayama-Yoshida, *Phys. Rev. B*. **1999**, 57, 9642.
- [35] K. Ueda, T. Maeda, T. Wada, *Thin Solid Films*. **2017**, 633, 23.
- [36] T. Maeda, W. Gong, T. Wada, *Curr. Opin. Green Sustain. Chem.* **2017**, 4, 77.
- [37] J. C. Mikkelsen, *Mater. Res. Bull.* **1977**, 12, 497.
- [38] I. A. Ivashchenko, I. V. Danyliuk, I. D. Olekseyuk, V. V. Halyan, *J. Solid State Chem.* **2014**, 210, 102.
- [39] R. S. Feigelson, R. K. Route, *Mat. Res. Bull.* **1990**, 25, 1503.
- [40] C. Rincón, S. M. Wasim, G. Marín, J. M. Delgado, J. R. Huntzinger, A. Zwick, J. Galibert, *Appl. Phys. Lett.* **1998**, 73, 441.
- [41] R. Caballero, V. Izquierdo-Roca, X. Fontané, C. A. Kaufmann, J. Álvarez-García, A. Eicke, L. Calvo-Barrio, A. Pérez-Rodríguez, H. W. Schock, J. R. Morante, *Acta Mater.* **2010**, 58, 3468.
- [42] J. Keller, O. V. Bilousov, E. Wallin, O. Lundberg, J. Neerken, S. Heise, L. Riekehr, M. Edoff, C. Platzer-Björkman, *Phys. Status Solidi A* **2019**, 216, 1900472.
- [43] J. K. Larsen, O. Donzel-Gargand, K. V. Sopiha, J. Keller, K. Lindgren, C. Platzer-Björkman, M. Edoff, *ACS Appl. Energy Mater.* **2021**, 4, 1805.
- [44] J. H. Boyle, B. E. McCandless, W. N. Shafarman, R. W. Birkmire, *J. Appl. Phys.* **2014**, 115, 223504.
- [45] C. J. Hages, N. J. Carter, R. Agrawal, *J. Appl. Phys.* **2016**, 119, 014505.
- [46] T. Kato, J. Wu, Y. Hirai, H. Sugimoto, V. Bermudez, *IEEE J. Photovoltaics*. **2019**, 9, 325.
- [47] S. Hegedus, W. N. Shafarman, *Prog. Photovolt. Res. Appl.* **2004**, 12, 155.
- [48] R. Scheer, H.-W. Schock, *Chalcogenide Photovoltaics*, Wiley-VCH Verlag, Weinheim **2011**.
- [49] I. L. Eisgruber, J. E. Granata, J. R. Sites, J. Hou, J. Kessler, *Sol. Energy Mater. Sol. Cells*. **1998**, 53, 367.
- [50] M. Eron, *J. Appl. Phys.* **1986**, 60, 2133.
- [51] M. Köntges, R. Reineke-Koch, P. Nollet, J. Beier, R. Schaffler, J. Parisi, *Thin Solid Films*. **2002**, 404, 280.
- [52] F. Liu, C. Yan, K. Sun, F. Zhou, X. Hao, M. A. Green, *ACS Photonics*. **2017**, 4, 1684.
- [53] S. Ravishankar, T. Unold, T. Kirchartz, *Science (Technical Comments)*. **2021**, 10, 1126.
- [54] P. D. Paulson, R. W. Birkmire, W. N. Shafarman, *J. Appl. Phys.* **2003**, 94, 879.
- [55] S. Minoura, T. Maekawa, K. Kadera, A. Nakane, S. Niki, H. Fujiwara, *J. Appl. Phys.* **2015**, 117, 195703.
- [56] A. Koprek, P. Zabierowski, M. Pawlowski, L. Sharma, C. Freysoldt, B. Gault, R. Wuerz, O. Cojocaru-Mirédin, *Sol. Energy Mater. Sol. Cells*. **2021**, 224, 110989.
- [57] H. J. Ko, G. H. Lee, H. J. Kim, M. S. Han, C. H. Jeong, J. H. Lee, H. S. Kim, J. H. Kim, K. B. Kim, S. H. Lee, *J. Cryst. Growth*. **2011**, 322, 91.
- [58] A. Virtuani, E. Lotter, M. Powalla, U. Rau, J. H. Werner, M. Acciarri, *J. Appl. Phys.* **2006**, 99, 014906.
- [59] A. Gerhard, W. Harneit, S. Brehme, A. Bauknecht, U. Fiedeler, M. C. Lux-Steiner, S. Siebentritt, *Thin Solid Films*. **2001**, 387, 67.
- [60] S. Siebentritt, L. Gütay, D. Regesch, Y. Aida, V. Deprédurand, *Sol. Energy Mater. Sol. Cells*. **2013**, 119, 18.
- [61] S. Nomura, J. Itoh, T. Takizawa, *Jpn. J. Appl. Phys.* **1993**, 32, 97.
- [62] M. Malitckaya, H. P. Komsa, V. Havu, M. J. Puska, *Adv. Electron. Mater.* **2017**, 3, 1600353.
- [63] B. L. Kronik, D. Cahen, H. W. Schock, *Adv. Mater.* **1998**, 10, 31.
- [64] S.-H. Wei, S. B. Zhang, A. Zunger, *J. Appl. Phys.* **1999**, 85, 7214.
- [65] D. W. Niles, K. Ramanathan, F. Hasoon, R. Noufi, B. J. Tielsch, J. E. Fulghum, *J. Vac. Sci. Technol. A Vacuum, Surf. Film* **1997**, 15, 3044.
- [66] Z. K. Yuan, S. Chen, Y. Xie, J. S. Park, H. Xiang, X. G. Gong, S. H. Wei, *Adv. Energy Mater.* **2016**, 6, 1601191.
- [67] F. Werner, D. Colombara, M. Melchiorre, N. Valle, B. El Adib, C. Spindler, S. Siebentritt, *J. Appl. Phys.* **2016**, 119, 173103.
- [68] H. Aboulfadl, K. V. Sopiha, J. Keller, J. K. Larsen, J. J. S. Scragg, C. Persson, M. Thuvander, M. Edoff, *ACS Appl. Mater. Interfaces* **2021**, 13, 7188.
- [69] S. Levchenko, N. N. Syrbu, A. Nateprov, E. Arushanov, J. M. Merino, M. León, *J. Phys. D: Appl. Phys.* **2006**, 39, 1515.
- [70] T. Negami, N. Kohara, M. Nishitani, T. Wada, T. Hirao, *Appl. Phys. Lett.* **1995**, 67, 825.
- [71] O. Yarema, M. Yarema, V. Wood, *Chem. Mater.* **2018**, 30, 1446.
- [72] O. Yarema, M. Yarema, D. Bozyigit, W. M. M. Lin, V. Wood, *ACS Nano* **2015**, 9, 11134.
- [73] H. Ishizaki, K. Yamada, R. Arai, Y. Kuromiya, Y. Masatsugu, N. Yamada, T. Nakada, *Mater. Res. Soc. Symp. Proc.* **2005**, 865, F5.12.
- [74] T. Maeda, W. Gong, T. Wada, *Jpn. J. Appl. Phys.* **2016**, 55, 04ES15.
- [75] J. Keller, O. V. Bilousov, J. Neerken, E. Wallin, N. M. Martin, L. Riekehr, M. Edoff, C. Platzer-Björkman, *Sol. RRL* **2020**, 4, 2000248.
- [76] I. Khatri, H. Fukai, H. Yamaguchi, M. Sugiyama, T. Nakada, *Sol. Energy Mater. Sol. Cells* **2016**, 155, 280.
- [77] S. Ishizuka, N. Taguchi, P. J. Fons, *J. Phys. Chem. C* **2019**, 123, 17757.



- [78] H. Tangara, S. Zahedi-Azad, J. Not, J. Schick, A. Lafuente-Sampietro, M. M. Islam, R. Scheer, T. Sakurai, *J. Appl. Phys.* **2021**, 129, 183108.
- [79] S. Ishizuka, N. Taguchi, J. Nishinaga, Y. Kamikawa, S. Tanaka, H. Shibata, *J. Phys. Chem. C* **2018**, 122, 3809.
- [80] M. A. Green, *Prog. Photovolt. Res. Appl.* **2009**, 17, 57.